Earthquake Engineering, Tenth World Conference © 1992 Balkema, Rotterdam. ISBN 90 5410 060 5

Low-cycle fatigue resistance of welded joints of high-strength steel under earthquake loading

H. Kuwamura
University of Tokyo, Japan

T. Suzuki
Nippon Steel Corporation, Futtsu, Japan

ABSTRACT: A heat-treated 600-MPa tensile-strength grade steel with yield ratios not more than 80 %, which has been newly produced by recent development of steel production practice in rolling mills, is examined in this study. Cyclic performance of the beam-to-column welded joints is investigated on the basis of low-cycle fatigue test, from which the relations between deformation amplitude and total energy absorption capacity exerted before fatigue fracture are determined. Comparing this fatigue resistance with the earthquake load input to the beam-to-column joints of building frames obtained from dynamic response analysis, the safety of the welded joints is estimated.

1 INTRODUCTION

It has been recognized that since high-strength steels with tensile-strength greater than 600-MPa have relatively high yield ratios as shown in Figure 1, such high-strength steels are not adequate for earthquake-resistant buildings whose structural safety is assured by ductile performance of the steel members. In fact, such high-strength steels have rarely been used in building construction practices of Japan.

Recent development of steel production practice, however, has realized a new type of high-strength steel characterized by its low yield ratio (Ohashi et al. 1990). This steel is a heat-treated 600-MPa tensile-strength grade steel with yield ratios not more than 80 % as indicated by the shaded part in Figure 1. It has been demonstrated in many aspects that structural members built from this new steel exhibit greater ductility than conventional quenched and tempered high-strength steels (Kuwamura 1988, Kuwamura & Kato 1989).

However, one of the problems involved in this new steel is that the material strength is reduced in the heat affected zones of welded joints, because this steel is a heat-treated product in the mill process. This concern is especially imposed on the behavior of beam-to-column welded joints where maximum stresses are cyclically introduced during earthquake motions. Thus, the safety of the welded joints should be verified on the basis of low-cycle fatigue test and structural response analysis.

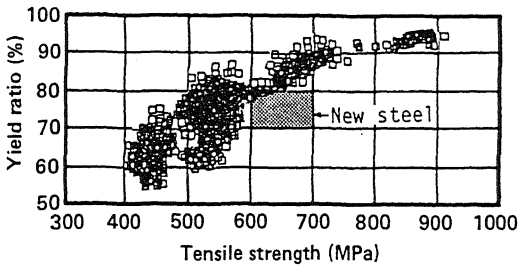

Figure 1. Relation between tensile strength and yield ratio of structural steels (Kuwamura & Kato 1989).

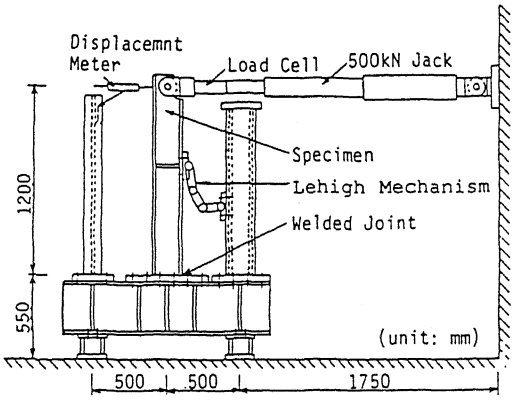

Figure 2. Apparatus for low-cycle fatigue test.

2 LOW-CYCLE FATIGUE TEST

2.1 *Test Scheme*

Each of seven specimens employed in this study is set up as a cantilever as shown in Figure 2. Horizontal force Q is cyclically applied at the free end by means of an oil jack of 500-kN capacity. Horizontal displacement δ is measured by a displacement meter fixed on an unmovable strut. A Lehigh mechanism supported by a

Table 1. Mechanical properties of the tested steel.

σ_y (MPa)	σ_u (MPa)	YR (%)	ε_u (%)	EL (%)
431	588	73.3	13.5	33.8

σ_y = lower yield stress
σ_u = tensile strength
YR = yield ratio, σ_y/σ_u
ε_u = uniform elongation
EL = total elongation in 50 mm

Table 2. Chemical composition of the tested steel. (weight %)

C	Si	Mn	P	S	Ceq	Pcm
0.148	0.178	1.11	0.011	0.004	0.34	0.21

$$Ceq = C + \frac{Si}{24} + \frac{Mn}{6} + \frac{Ni}{40} + \frac{Cr}{5} + \frac{Mo}{4} + \frac{V}{14}$$

$$Pcm = C + \frac{Si}{30} + \frac{Mn}{20} + \frac{Ni}{60} + \frac{Cr}{20} + \frac{Mo}{15} + \frac{V}{10} + \frac{Cu}{20} + 5B$$

sufficiently stiff strut is attached to the specimen at the midheight in order to prevent lateral buckling of the specimen.

The specimens have a welded H-shaped section of H-200x100x9x9mm. Mechanical properties and chemical composition of the 9-mm thick steel plate built in the specimens are shown in Tables 1 and 2, respectively.

The welding details of the specimen connected to the bottom end plate are shown in Figure 3. The welding was done by CO_2 semi-automatic arc welding using seamless flux cored wires of 600-MPa tensile strength proof. Each flange joint is full penetration weld with a single bevel groove blocked by flux backing plates which were removed after welding. Thus, no back chipping was employed and only reinforcing fillet weld was deposited for the back welding. The web joint was fillet weld without scallops. Two levels of heat input were applied at the flange weld, because the mechanical properties in the heat affected zone may be influenced by the amount of heat input. The selected levels were 20 kJ/cm (normal) and 60 kJ/cm (abnormally large), which were practiced by flat and vertical welding positions, respectively.

The cyclic loads were applied in the manner of a constant displacement range chosen from $\pm 3\delta_p$, $\pm 4\delta_p$, $\pm 5\delta_p$, and $\pm 7\delta_p$, where δ_p is the calculated elastic displacement at the full plastic load Q_p. The values of δ_p and Q_p are common to all the specimens.

2.2 *Test results*

All of the specimens collapsed due to fatigue fracture in almost the same fashion. An initial crack, which was visually observed, took place at the toe of the projected flange edge, and gradually propagated into the flange center in the transverse direction as shown in Figure 4.

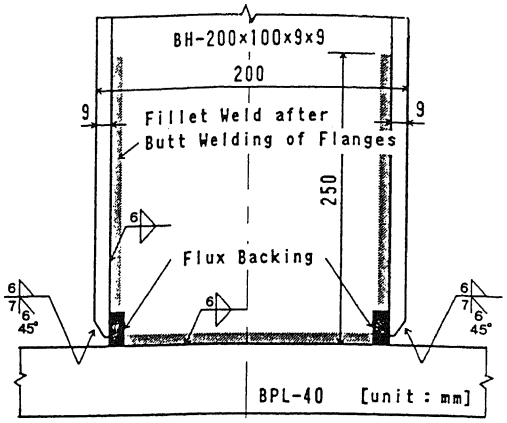

Figure 3. Welding details of low-cycle fatigue specimens.

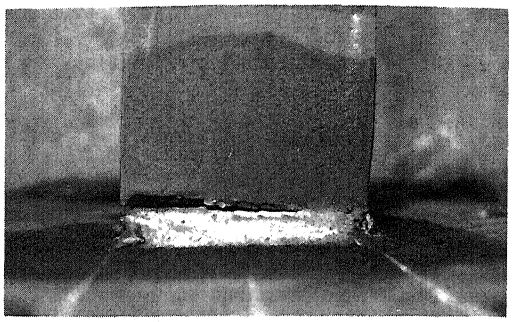

Figure 4. Fatigue crack at the final stage of loading.

Finally, the crack reached the web plate, and then restoring force was abruptly lost.

The hysteresis curves obtained from the test are shown in Figure 5. In this figure, symbol ▽ indicates the final fracture at which abrupt unloading took place, a_o is the displacement amplitude, N_f is the number of cycles experienced before the fracture, and W_f is the total energy absorption accumulated before the fracture only in the side of loading direction in which the final fracture occurred. Each specimen is designated by a symbol like 3-F, in which the first digit indicates the displacement amplitude and the second character indicates the welding position, i.e., Flat or Vertical, related to the amount of heat input.

Major properties of the specimens' performance obtained from the low-cycle fatigue test are shown in Table 3, in which N is the number of cycles, W is the cumulative energy absorption, μ is the average ductility, and η is the cumulative ductility, and subscripts c and f denote crack initiation and fracture, respectively, in relation to the base properties. The crack initiation is based on visual observation. The average ductility μ and cumulative ductility η are defined in the manner illustrated in Figure 6. All properties with subscript c are calculated only in the side of loading direction in which the first crack is observed. Likewise, all properties with subscript f are

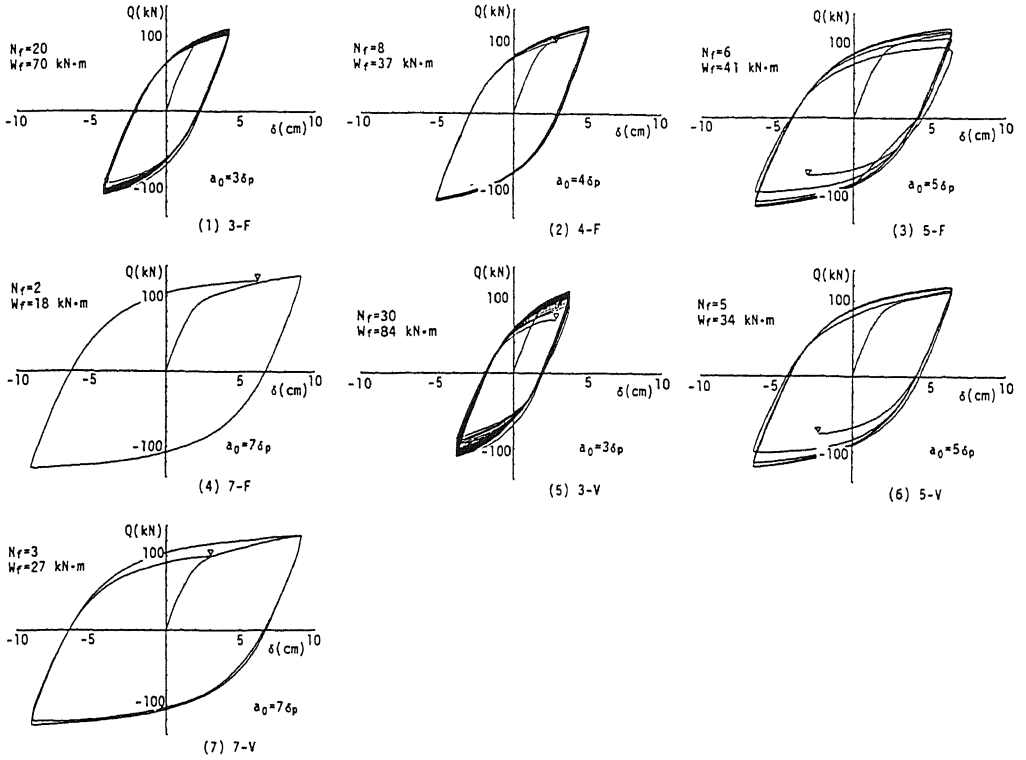

Figure 5. Hysteresis curves obtained from low-cycle fatigue test.

Table 3. Major properties obtained from low-cycle fatigue test

	crack initiation				final fracture			
Specimen	N_c	W_c	μ_c	η_c	N_f	W_f	μ_f	η_f
3-F	13	46	5.3	45	20	70	5.3	69
4-F	3	14	5.8	13	8	37	6.1	37
5-F	2	15	8.8	15	6	41	8.3	40
7-F	1	7.5	7.5	7.3	2	18	8.9	17
3-V	11	31	4.5	30	30	84	4.7	82
5-V	2	16	8.8	16	5	34	8.1	33
7-V	1	7.4	7.5	7.2	3	27	9.4	26

Unit of W_c and W_f : kN-m.

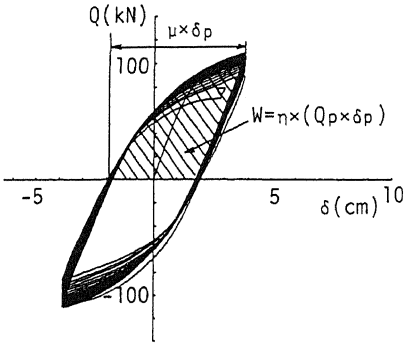

Figure 6. Definition of the performance properties, W, μ, and η in low-cycle fatigue test.

determined only in the side of loading direction in which fracture took place.

The relations between average ductility and cumulative ductility obtained from the test are shown in Figure 7. The most significant feature observed from this figure is that the cumulative ductility, in other words the energy absorption capacity, decreases with the increase in the average ductility for both phases of crack initiation and fracture. This may be explained by the increased contribution of Bauschinger effect in smaller amplitude displacement cycles. In addition, there seems no apparent influence of heat input on the fatigue resistance. Thus, the following empirical formulae may be obtained from applying the method of least squares to the test data:

$$\eta_c = 360\,\mu_c^{-1.65} \quad \text{for crack initiation} \qquad \text{.....(1)}$$

$$\eta_f = 1140\,\mu_f^{-1.73} \quad \text{for fracture} \qquad \text{.....(2)}$$

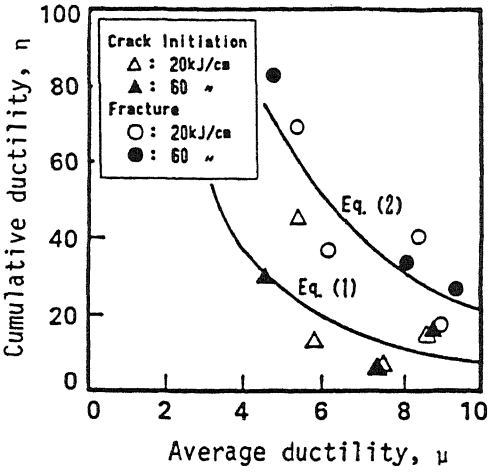

Figure 7. μ vs. η obtained from low-cycle fatigue test.

3 EARTHQUAKE RESPONSE ANALYSIS

3.1 *Structural models*

Any welded joint, whatever excellent workmanship is employed, eventually suffers fatigue fracture under cyclic loading. However, the load input produced by earthquake motion is not infinite. Thus, the important thing in design is to let the welded joint survive the earthquake with an ultimate but finite intensity. Such load input may be calculated from structural response analysis, in which the seismic intensity is adequately scaled to meet the ultimate design specification.

In this study, seismic load input at the welded joints of beam ends in a rigid frame with one bay and eight stories is examined. The member strengths were proportioned according to the seismic force distribution over the building height prescribed by the current design code of Japan. However, since the code does not specify the failure mode, many choices of strength proportioning with different failure modes are possible. Here, 13 frame models as shown in Figure 8 are selected. In the modes represented by $n = 2$, only one beam is involved in the failure interstories, which may cause maximum damage in the beam ends, because other beams and most columns remain elastic. The mode represented by $n = 8$ is the overall collapse mechanism in that all beams are involved in the failure stories, which may minimize the damage in each beam end. The mode represented by $n = 4$ may be an intermediate case.

The response analysis was performed on the basis of plastic hinge method in that each structural member is elastic and every member's end is connected to a rigid-plastic spring whose hysteresis behavior example is shown in Figure 9. In the case of Figure 9, the numbers of plastic excursions in the plus and minus loadings represented by N_{p+} and N_{p-}, respectively, are calculated as $N_{p+} = 2$, $N_{p-} = 1$, the cumulative ductilities are $\eta_+ = 10$ and $\eta_- = 5$, and the average ductilities defined as $\eta / N_p + 1$ are $\mu_+ = 6$ and $\mu_- = 6$.

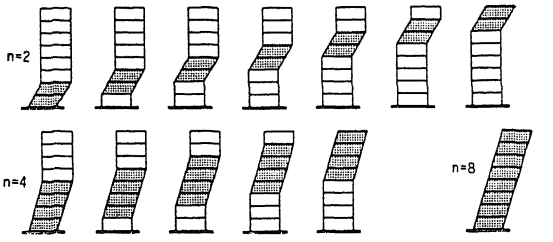

Figure 8. Failure mechanisms of the examined 13 structural frames under static horizontal seismic forces.

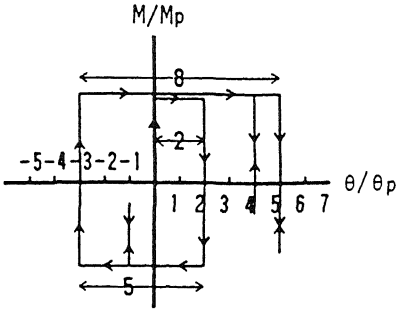

Figure 9. Illustration of hysteresis curves of a rigid-plastic spring incorporated in the frames for response analysis.

3.2 *Earthquake motions*

The earthquake accelerations employed in the analysis are El Centro, NS, 1940 and Hachinohe EW, 1968 as shown in Table 4. These accelerations were factored such that the energy input is equivalent to that specified in Japan seismic design code, which is realized by the following factor (Kuwamura & Galambos 1988):

$$\beta = \frac{2V_{Eo}}{\sqrt{I_E \cdot T_o}} \tag{3}$$

where V_{Eo} is the upper bound of the energy-based velocity spectrum which is equated to 200 cm/sec in this case to meet the load intensity of the code-specified ultimate earthquake, I_E is the integral of the squared acceleration, or acceleration power, of the original motion, and T_o is the predominant period.

3.3 *Results of response analysis*

Dynamic behaviors of the 13 model frames shown in Figure 8 were analyzed under the two earthquake excitations with factored accelerations given in Table 4. All of the hysteresis curves of the rigid-plastic springs attached to the beam ends involved in the designated interstory failure indicated by the shades in Figure 8 were picked up, and their average ductilities and cumulative ductilities, whose calculation was previously described and illustrated in Figure 9, are plotted in Figures10a, 10b, and 10c, corresponding to the number

Table 4. Earthquake motions used for response analysis.

Earthquake motion	data length (sec)	a_{max} (gal)	I_E (cm²/sec³)	T_o (sec)	$\frac{\sqrt{I_E T_o}}{2}$ (cm/sec)	β
El Centro NS, 1940	10.0	342	75,100	0.55	102	1.95
Hachinohe EW, 1968	20.0	204	65,300	0.90	121	1.65

a_{max} = peak acceleration in the original accelerogram

$I_E = \int_0^{t_o} a^2\, dt$ =acceleration power of the original motion

T_o = predominant period

β = amplification factor to the original acceleration

of failure stories n =2, 4, and 8, respectively. It is obvious from comparing these figures that the ductility response, in other words ductility demand, is smaller for the frame with a larger n. When the structural members' strengths are adequately proportioned to achieve the overall failure mechanism, or the weak-beam strong-column frame, the average ductility response and the cumulative ductility response at the beam ends may be less than 3 and 8, respectively as observed in Figure 10c. However, when the frame fails in local modes, the beam ends may suffer larger damage, e.g., average ductility of 4 and cumulative ductility of 20 in this case as observed in Figure 10a.

4 SAFETY ESTIMATION

The load input in terms of average ductility and cumulative ductility shown in Figures 10a, 10b, and 10c is wholly collected and plotted again in Figure 11. The data are distributed in the range of $\mu \leq 4$ and $\eta \leq 20$. The low-cycle fatigue resistance of the welded joints at the stage of fracture shown in Figure 7 is plotted again in the same figure. It is observed in Figure 11 that the resistance is distributed in a farther distant area from the origin of the coordinate system than the load input. Thus, the welded joints have enough safety against the risk of fatigue fracture under the earthquake motion of the code-prescribed ultimate intensity.

5 CONCLUSIONS

The safety of beam-to-column welded joints under a strong earthquake is investigated for 600-MPa tensile-strength grade steel incorporated into rigid frames. Comparing low-cycle fatigue resistance of the joints and earthquake load input into the joints in terms of average and cumulative ductilities, it was found that the joints have an enough safety margin against a strong earthquake motion having the ultimate intensity prescribed in Japanese seismic design code. However, it should be noticed that these results are based on the following

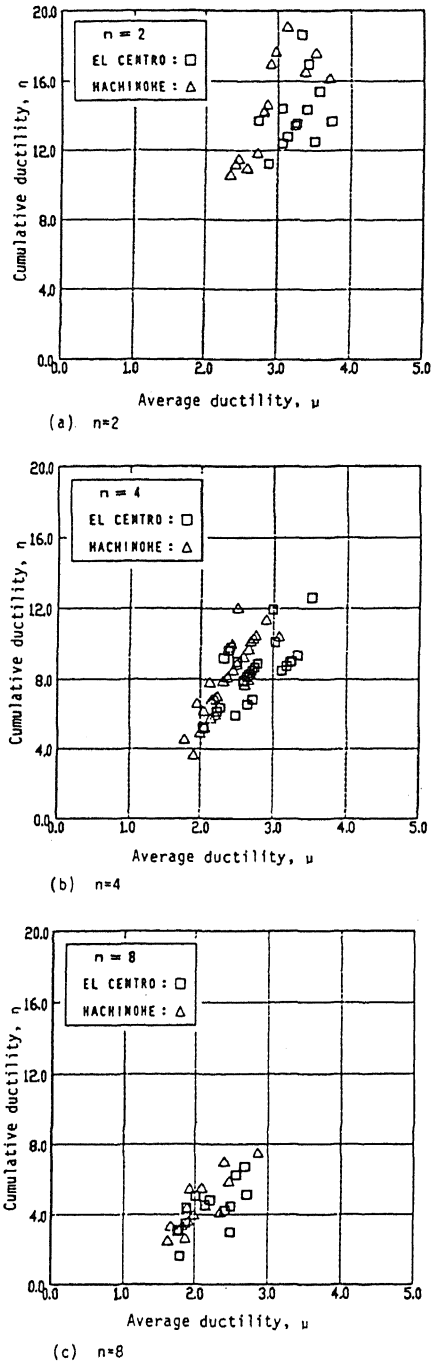

Figure 10. μ vs. η obtained from response analysis (a) n =2, (b) n =4, (c) n =8.

simplifications: rather idealized welding details without scallops were employed, a small size of beam section was used, and constant or average displacement amplitudes were applied instead of variable amplitudes. Further studies including large scales of specimens and

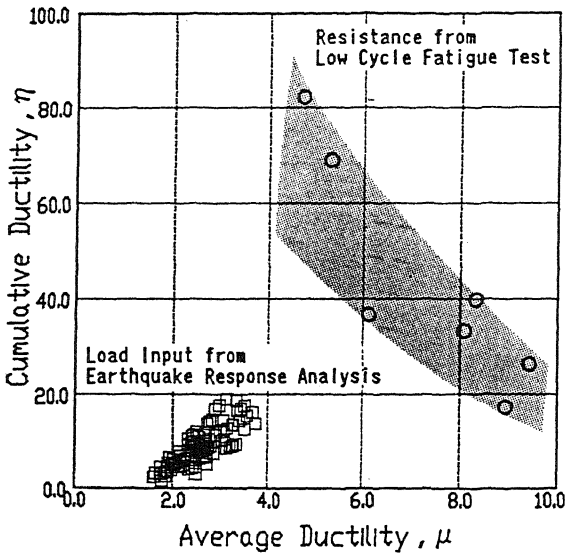

Figure 11. Comparison of low-cycle fatigue resistance and earthquake load input in beam-to-column joints.

loading schemes of variable displacement range may be necessary.

REFERENCES

Ohashi, M. et al. 1990. Development of New Steel Plates for Building Structural Use, *Nippon Steel Tech. Report*, No.44, pp.8-20.

Kuwamura, H. 1988. Effect of yield ratio on the ductility of high-strength steels under seismic loading, *Proc. of SSRC*, Minneapolis, pp.201-210.

Kuwamura, H. & Kato, B. 1989. Inelastic Behaviour of high strength steel members with low yield ratio, *PSSC Papers*, Gold Coast, pp.429-437.

Kuwamura, H. & Galambos, T.V. 1988. Earthquake load effect for structural risk assessment, *Proc. 9WCEE*, Tokyo-Kyoto, V, pp.313-318.